2007

Electrowetting at the nanoscale

C. D. Daub

D. Bratko
Virginia Commonwealth University, dbratko@vcu.edu

K. Leung

A. Luzar

Electrowetting at the nanoscale

Christopher D. Daub[1], Dusan Bratko[1,2], Kevin Leung[3], and Alenka Luzar[1,*]

Department of Chemistry, Virginia Commonwealth University, Richmond, Virginia USA, 23284, Department of Chemical Engineering, University of California, Berkeley, California USA, 94720 and Sandia National Laboratories, MS 1421, Albuquerque, New Mexico USA, 87185

TOC graphic:

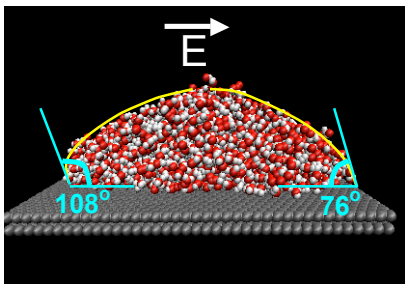

[1] Department of Chemistry, VCU

[2] Department of Chemical Engineering, UC Berkeley

[3] Sandia National Laboratories

[*] Corresponding author. email: aluzar@vcu.edu

Abstract

Using molecular simulations of nano-sized aqueous droplets on a model graphite surface we demonstrate remarkable sensitivity of water contact angles to the applied electric field polarity and direction relative to the liquid/solid interface. The effect is explained by analyzing the influence of the field on interfacial hydrogen bonding in the nanodrop, which in turn affects the interfacial tensions. The observed anisotropy in droplet wetting is a new nanoscale phenomenon that has so far been elusive as, in current experimental setups, surface molecules represent a very low fraction of the total number affected by the field. Our findings may have important implications for the design of electrowetting techniques in fabrication and property tuning of nanomaterials.

Electric field effects on water interfacial properties abound, ranging from electrochemical cells, to nanofluidic devices, to membrane ion channels. Electric fields are useful in regulating macroscopic properties including wettability, adhesion and friction for microfluidics[1,2] and in applications such as electrowetting on dielectric (EWOD).[3] Recent experiments[4–7] investigated the effect of electric field on contact angle, which also potentially impacts the stability of liquid-liquid interfaces,[8] and may be pertinent to carbon nanotube sieves of O(1 μm) thickness.[9] There is current interest in understanding the effect of electric field on interfacial properties of water,[10–12] since comparatively large electric fields (with $\mathbf{E} \cdot \boldsymbol{\mu}$, $\mathbf{E}$ being the electric field vector and $\boldsymbol{\mu}$ the dipole moment vector, not negligible compared to $k_B T$) may exist in and influence transport properties of the ion channels of cell membranes.[13] They are also important in membrane electroporation[14,15] and play a role at the active site of an enzyme.[16]

A property central to interfacial thermodynamics is the contact angle θ_c, which determines whether the surface de-wets ($\theta_c > 90°$) or wets ($\theta_c < 90°$) according to the Young equation,

$$\cos\theta_c = (\gamma_{sv} - \gamma_{sl})/\gamma_{lv}, \tag{1}$$

where $\gamma_{\alpha\beta}$ are the interfacial free energies of the three phases, solid (s), liquid (l), and vapor (v). If the drop is small, the line tension τ[17] also plays a role, $\cos\theta_c(r_B) = \cos\theta_\infty - \tau/\gamma_{lv} r_B$, where r_B is the base radius of the drop.[18]

In macroscopic systems, an electric field typically reduces the contact angle. In the usual EWOD setup, a conducting water drop spreads into a weak electric field $\mathbf{E}$. In pure water, an ion concentration of 10^{-7} M leads to a double layer of thickness $\sim 10^3$ nm at the capacitor-liquid interface, restricting the field to an interfacial layer of thickness $D \sim 1$ μm at the base of the drop. In such cases the contact angle can be described by the well-known Young-Lippmann equation

$$\cos\theta_c = \cos\theta_c^0 + \frac{\langle \epsilon\epsilon_0 |\mathbf{E}|^2 \rangle D}{2\gamma_{lv}}. \tag{2}$$

Here, the brackets denote the average over D; θ_c and θ_c^0 are the contact angles with and without the electric field, respectively, ϵ is the dielectric constant inside the layer and ϵ_0 is the permittivity of free space.

Unlike macroscopic drops,[19] water nanodroplets with size well under the Debye screening length, when placed between plates of a capacitor, essentially

behave as insulators. The field, although screened by water polarization, permeates the whole droplet. Polarization is strongest at liquid surfaces.[20] Dipolar molecules may therefore be attracted to the interface, reducing interfacial free energies. The average interaction, w, between a free dipole $\boldsymbol{\mu}$ and an external field $\mathbf{E}$ is $w \sim -|\mathbf{E}||\boldsymbol{\mu}|L(|\mathbf{E}||\boldsymbol{\mu}|/kT) \rightarrow -|\boldsymbol{\mu}|^2|\mathbf{E}|^2/3kT$ in weak field, where $L(x)$ is the Langevin function. This suggests surface free energies and contact angle should depend only on the absolute strength of the field regardless of its direction, a picture consistent with Eq. 2 and its generalizations.[6]

Possible changes in bare surface tensions due to the alignment of surface molecules in the field, however, can further affect the contact angle, especially for small droplets with comparatively high populations of molecules residing at the surface.[5] While such situations can be common in ion channels and nanoporous materials, they are hard to observe in a typical experimental setup for measuring a macroscopic contact angle. Molecular simulations, however, are ideally suited for investigating interfacial phenomena at molecular scales, especially those of nanoscale systems.

In this Letter, we provide for the first time a molecular picture of aqueous nanodroplets spreading on a model apolar (graphite) surface subject to a field inside a capacitor. Our setup (see Fig. 1) has been realized in experiments,[4,5] albeit on longer lengthscales. The advantage of studying the contact angle dependence on the electric field is that it is a direct, unambiguous measure of field effect on wettability of the surface at the simulation conditions. The electric field in our simulations (0.03 V/Å) is similar to local fields inside ion channels.[21] We consider fields perpendicular to the surface with both positive and negative polarities, as well as a field applied parallel to the surface, a situation also found in nature *e.g.* in an ion channel.

Potential models. We apply the Extended Simple Point Charge (SPC/E) model[22] for water and the accurate water-graphite interactions of Werder *et al.*[23] In general, external fields may polarize water molecules suggesting the use of polarizable models of water. The field strength we apply is, however, very weak compared to molecular or ionic fields, where polarizable potentials become necessary. As illustrated in Fig. 6 of Ref. 24, polarization of a water molecule by the external field becomes negligible below field strengths of ~ 1 V/Å. Neglect of water polarizability is therefore not expected to visibly modify the response to applied field at the field strength we study.

Simulation methodology. Water drops containing 2000 molecules are simulated interacting with two layers of graphite, staggered as in crystalline graphite, with an interlayer spacing of 3.4 Å. The simulation box is a rectangular prism, with box edges $L_x = 117.9$ Å, $L_y = 119.1$ Å and $L_z = 200.0$ Å, and periodic boundary conditions are imposed throughout. In order to speed up the calculation, the graphite layers are frozen in place during the simulation and the SHAKE algorithm is used to maintain the internal geometry of the water molecules. We performed the simulations in the NVT ensemble, using a Nosé-Hoover thermostat with a 100 fs time constant to keep the temperature fixed at 300 K. The simulation timestep was 1 fs. The LAMMPS 2001 code[25] was used, modified to accomodate the effect of the electric field. The imposed electric field $\mathbf{E}_0$ is uniform. $\mathbf{E} < \mathbf{E}_0$ is adequately represented by the sum of $\mathbf{E}_0$ and the implicit field $\mathbf{E}_{pol}$ contributed by all molecular partial charges in the specified configuration.

Drop analysis. We have adapted the technique developed by Werder *et al.*[23,26–28] for determination of the contact angle, which basically entails fitting the cross-section of the droplet to a truncated circle. In the presence of the electric field, the drop can no longer be assumed to be spherical. In an electric field applied perpendicular to the surface, the radial profile of the drop is still symmetric, but we fit the vertical drop cross-section to an ellipse instead. In the electric field parallel to the surface, the radial profile is no longer symmetric. θ_c varies with the angle, ϕ between the field vector and the vector from the center of mass to the given position around the drop. Since deviations from spheroidal shape, observed in the vicinity of the three-phase contact line signify the departure from apparent macroscopic behavior, we estimate the microscopic analogue of the contact angle by considering only the spheroidal portion of the droplet contour. In doing so, we ignore the noncompliant region[23] near the contact line that comprises the transition from the unperturbed Young angle[29] to the apparent global value. Empirically, the size of this region corresponds to between 2-3 molecular diameters,[23] consistent with our observations (Fig. 2).

Electric field effect on nanodroplet shape. Experimentally[3] and from continuum simulation[19,30] it is known that a water drop spreads on the surface under the influence of the electric field. This behaviour is replicated in our simulated nanodroplets. In Figure 1 we show snapshots of the drop generated during the molecular dynamics simulations in all three of the situations we study. It can

be seen that the most visible effect of the electric field is to stretch out the drop along the direction of the applied field, in agreement with experimental findings.[4,5]

Electric field effect on contact angle. Macroscopic thermodynamics predicts (Eq. 2) the lowering of contact angle in electric field. In Figure 2 we show the points of the vertical cross section and the fitted circle or ellipse to the cross section without field and in both parallel and perpendicular fields.

Perpendicular field. Results in the perpendicular field are shown in Table 1. The contact angle is lowered in all cases studied. The overall increase in wettability agrees with thermodynamic arguments[31] and predictions for various water droplet and water slab scenarios.[6] However, the polarity plays a substantial role, with the positive electric field producing a reproducibly lower contact angle than the negative field. This demonstrates that there is a bias against molecular orientations with the oxygen atom pointing away from the solid surface. Our observations conform with experimentally observed sign preference for ion induced droplet nucleation.[32,33] Independent of any other effects, the stretching of the drop in the perpendicular electric field tends to bring the contact angle closer to 90°. Depression of θ_c below 90° shows that the stretching effect alone does not dominate the field dependence of the contact angle.

There is also a difference between polarities in the amount of droplet stretching observed, with the negative field producing a drop height ~ 2 Å higher than the positive field. Our simulations of a free drop in electric field (not shown) reveal reproducible asymmetry as well. There is a difference in curvatures on opposite droplet tips, the curvature being lower at the "leading" edge (in the direction of the field vector) and higher at the "trailing" edge. The difference is consistent with, but smaller than that observed in the sessile droplet of similar size in perpendicular field.

Parallel field. Even more pronounced asymmetry is seen in the sessile droplet in an electric field parallel to the graphite surface. At the "leading" edge of the drop ($\phi = 0°$), the contact angle is determined to be $\theta_c = 76.3 \pm 4.5°$. θ_c increases as one goes around the drop, rising to $93.6 \pm 1.5°$ at $\phi = 90°$ (the same as the contact angle with no applied field), and up to $107.6 \pm 5.5°$ at the "trailing" edge of the drop. In analogy with the previous result, the electric field tends to stretch the droplet out along the direction of the field (Fig.2).

Electric field effect on interfacial orientational profiles. Water molecules

tend to realign in the applied field, competing with orientational preferences of water molecules relative to the graphite surface and the liquid-vapor interface. Such preferences, associated with anisotropic water-water interactions, are known from studies in field-free systems.[34–36] We have collected distributions of the dipole moment vectors $\boldsymbol{\mu}$, as well as the OH bond vector, $\vec{\mathrm{OH}}$.[35,37,38] The orientational distributions for the solid-liquid interface in different fields are displayed in Figure 3. As expected, in the absence of field, the distributions of $\boldsymbol{\mu}$ peak at dipole orientations parallel to the interface. Under applied field, a shift reflecting partial alignment is observed. The alignment is more pronounced for negative perpendicular field compared to the positive one. This is consistent with the depletion of hydrogen bonds (Table 2) in the surface layer subject to negative field. In the positive field, the hydrogen-bonding network is slightly enriched, explaining the weaker polarization of the surface layer in this case. Similar arguments apply to the $\vec{\mathrm{OH}}$ distributions. In the parallel field, no significant change is observed confirming that the normal component of each molecular dipole is virtually decoupled from the parallel field. Changing field direction has similar, albeit less striking, effects at the liquid/vapor interface (not shown).

Electric field effect on interfacial hydrogen bonding. Alignment of water molecules with the field will generally have an effect on hydrogen bonding between surface molecules,[34–36] and hence on γ_{sl} *and* γ_{lv}. We present the values of $\langle n_{HB} \rangle$, the mean number of hydrogen bonds per molecule, in all of the interesting interfacial regions of the drop: we have examined the solid-liquid interface in all cases, and the entire liquid-vapor interface in all but the parallel field, where we have instead calculated $\langle n_{HB} \rangle$ in the interface near the leading ($-90^\circ < \phi < 90^\circ$) and trailing ($90^\circ < \phi < 270^\circ$) edges of the drop, since here the liquid-vapor interface can be nearly perpendicular to the electric field.

As expected, the number of hydrogen bonds drops near the interfaces (see Table 2). The ratio of surface bonds to interior bonds is approximately 80%, close to previous theoretical[34–36] and experimental[37] estimates of approximately 75%. At the solid-liquid interface, we see that there are an additional 0.06 bonds/molecule in the positive perpendicular field and a *reduction* of 0.1 bonds/molecule in the negative field. Although absolute values of $\langle n_{HB} \rangle$ are somewhat sensitive to the hydrogen bond definition,[39,40] the *changes* in $\langle n_{HB} \rangle$ due to the applied field do not appreciably depend on the hydrogen bonding criteria. In macro-

scopic systems, reduction in $\langle n_{HB} \rangle$ of about one H bond translates to surface tension contribution of $\sim 45 \pm 5$ mN/m;[34] the difference $\Delta\langle n_{HB} \rangle \sim 0.15$ observed upon the reversal in field polarity can therefore have a strong effect on surface tensions γ_{sl} and γ_{lv}. Similar losses in hydrogen bonding are seen at the three-phase contact line, suggesting that the line tension is also affected by the electric field.

The value of the interfacial tension γ rises as the number of hydrogen bonds in the interface is lowered. Therefore, we can predict that γ_{sl} should be larger in a negative perpendicular field, and smaller in a positive field. Effects on hydrogen bonding and hence surface tensions are weaker for other field angles, including parallel field near the graphite. We note that this effect is not predicted by macroscopic thermodynamic theories (Eq. 2),[6] which assume that bare interfacial tensions remain unchanged in the electric field, and that the direction of the field is unimportant.

The hydrogen bond analysis also indicates that γ_{lv} will be smaller at the trailing edge. Since the difference $\gamma_{sl} - \gamma_{sv}$ is equally affected by the parallel field at both edges, then to the extent that Young's equation (Eq. 1) can be relied on, a smaller value of γ_{lv} should result in larger $|\cos\theta_c|$, and hence θ_c should depart further from 90°. For positive $\gamma_{sl} - \gamma_{lv}$ the contact angle should be higher at the trailing edge, as is indeed observed (Table 1). The directional dependence of the field's effect on the surface tension γ_{lv} also provides an incentive for the liquid-vapor interface at the leading and trailing edges to tilt away from the unfavorable normal angle relative to the field. This is seen as well in the asymmetry of the free droplet, as the trailing edge with smaller γ_{lv} will manifest greater curvature as a result of the lessened tendency to minimize surface area. This mechanism can contribute to the decrease of the apparent contact angle at the leading edge, and the increase in θ_c at the trailing edge. The above two effects work in concert, as the contact angle rises almost to 110° at the trailing edge. The lowering of the contact angle at the leading edge, while $\gamma_{sl} - \gamma_{sv} > 0$, can also partly be attributed to the droplet's distortion by the field (*vide supra*).

Analysis of the hydrogen bonding of surface water molecules allows us to make some general predictions about the effect of electric fields on nanodrop surface free energies γ_{lv} and γ_{sl}, with γ_{sl} *smaller* in the positive perpendicular field and *larger* when the field is reversed. Similarily, in a field applied parallel to the solid/liquid interface γ_{lv} will be larger at the leading edge of the drop, and

smaller at the trailing edge. The magnitude of these differences compared to the field-free drop is about equal and opposite for each edge, varying continuously around the drop which is no longer axially symmetric. Overall, the drop is stretched along the direction of the field as the water dipoles preferentially align with the field. In perpendicular field, this tends to bring the contact angle closer to 90°. Observed contact angle changes are consistent with these predictions.

In conclusion, in contrast with measurements in macroscopic systems and predictions from conventional, continuum analyses, our simulations reveal a *notable influence of field direction relative to the interfaces on the contact angle*. Transition to the nanoscale changes the determining factors of electrowetting, because molecular detail plays an important role. In particular it is the orientational bias of surface molecules that couples with the fluid's response to applied field. Depending on field direction, there can be synergy or interference between reorientational forces in the interfacial water and alignment with the field. Thus, our model calculations reveal a new nanoscale phenomenon that experimentalists have anticipated[5,41] but so far have been unable to detect because in a typical experimental setup the fraction of surface molecules is much smaller than in the nanoscale drop which we study.

Looking ahead, we can imagine two possible applications for interfacial engineering. We demonstrated that sessile water nanodroplets on a weakly hydrophobic surface (contact angle $\sim 90°$) can become "Janus" nanodrops[42–44] under the influence of an electric field, with water favorably attracted to the surface on one side (hydrophilic) but abhorred on the other side (hydrophobic). The idea of switchable wettability/hydrophobicity due to nano-electrowetting may open new doors for nanoscale research. Recently, excellent reports have been published on changing the macroscopic water contact angle only by altering the surface polarity or morphology, without alteration of the chemical properties of the surface, by various methods[45,46] including the use of photochromic compounds.[47] The slow switching time (hours to days)[47] and hysteresis,[45] however, pose current experimental challenges. By comparison, a real-world experimental manifestation of our computer simulation would have a near-instantaneous response, on the $O(10$ ps) time scale of water reorientation near a hydrophobic interface.[48] It would be interesting to study the effect of alternating field in a similar nanoscale setting to determine the highest frequency that would still have an impact. We will address this issue in future research.

Our second example of possible application is concerned with field-induced changes in material hydrophilicity relevant to water condensation and concomitant flashover discharge on polymer wire insulators. Since condensation is initiated by a nucleation process, the behaviour of a nanodroplet will impact the overall wetting process. Further, the deformation of droplets in an electric field has recently been implicated in the flashover mechanism.[30] The elongation of a drop in the field is well understood in macroscopic systems,[30,49] however upon descent to the nanoscale it must reflect molecular level details and mechanisms. The advent of micro- and nanoelectronics also implies the development of miniaturized insulating devices. The design of nanoscale insulators resistant to pollution malfunction requires understanding of electrowetting at the pertinent length scale.

Acknowledgement. We are grateful to Richard L. Jaffe, Jacob Klein and José Teixeira for helpful input. This work was supported by the National Science Foundation through CHE-0512131 and BES-0432625. We acknowledge NSF (CHE-060047) and Hewlett Packard for computational resources. Work at Sandia was supported by the Department of Energy under Contract DE-AC04-94AL85000. Sandia is a multiprogram laboratory operated by Sandia Corporation, a Lockheed Martin Company, for the U.S. DOE.

References

1. Squires, T. M.; Quake, S. R. *Rev. Mod. Phys.* **2005,** *77,* 977.
2. Robinson, L.; Hentzell, A.; Robinson, N. D.; Isaksson, J.; Berggren, M. *Lab Chip* **2006,** *6,* 1277.
3. Mugele, F.; Klingner, A.; Buehrle, J.; Steinhauser, D.; Herminghaus, S. *J. Phys.: Condens. Matter* **2005,** *17,* S559.
4. Bateni, A.; Susnar, S. S.; Amirfazli, A.; Neumann, A. W. *Langmuir* **2004,** *20,* 7589.
5. Bateni, A.; Laughton, S.; Tavana, H.; Susnar, S. S.; Amirfazli, A.; Neumann, A. W. *J. Colloid Interface Sci.* **2005,** *283,* 215.
6. Shapiro, B.; Moon, H.; Garrell, R. L.; Kim, C.-J. *J. Appl. Phys.* **2003,** *93,* 5794.
7. Quinn, A.; Sedev, R.; Ralston, J. *J. Phys. Chem. B* **2003,** *107,* 1163.
8. Daikhin, L. I.; Kornyshev, A. A.; Urbakh, M. *Chem. Phys. Lett.* **1999,** *309,* 137.
9. Holt, J. K.; Park, H. G.; Wang, Y. M.; Stadermann, M.; Artyukhin, A. B.; Grigoropoulos, C. P.; Noy, A.; Bakajin, O. *Science* **2006,** *312,* 1034.
10. Dzubiella, J.; Hansen, J.-P. *J. Chem. Phys.* **2005,** *122,* 234706.
11. Vaitheeswaran, S.; Rasaiah, J. C.; Hummer, G. *J. Chem. Phys* **2004,** *121,* 7955.
12. Vaitheeswaran, S.; Yin, H.; Rasaiah, J. C. *J. Phys. Chem. B* **2005,** *109,* 6629.
13. Bostick, D.; Berkowitz, M. L. *Biophys. J.* **2003,** *85,* 97.
14. Tieleman, D. P.; Leontiadou, H.; Mark, A. E.; Marrink, S.-J. *J. Am. Chem. Soc.* **2003,** *125,* 6382.
15. Tarek, M. *Biophys. J.* **2005,** *88,* 4045.
16. Suydam, I. T.; Snow, C. D.; Pande, V. S.; Boxer, S. G. *Science* **2006,** *313,* 200.

17. Wang, J. Y.; Betelu, S.; Law, B. M. *Phys. Rev. E* **2001,** *63,* 031601-1.

18. Widom, B. *J. Phys. Chem.* **1995,** *99,* 2803.

19. Walker, S. W.; Shapiro, B. *J. Microelectromech. Syst.* **2006,** *15,* 986.

20. Ballenegger, V.; Hansen, J. P. *J. Chem. Phys.* **2005,** *122,* 114711.

21. Eisenberg, R. private communication.

22. Berendsen, H. J. C.; Grigera, J. R.; Straatsma, T. P. *J. Phys. Chem.* **1987,** *91,* 6269.

23. Werder, T.; Walther, J. H.; Jaffe, R. L.; Halicioglu, T.; Koumoutsakos, P. *J. Phys. Chem. B* **2003,** *107,* 1345.

24. Yang, K.-L.; Yiacoumi, S.; Tsouris, C. *J. Chem. Phys.* **2002,** *117,* 337.

25. Plimpton, S. J. *J. Comp. Phys.* **1995,** *117,* 1.

26. Hautman, J.; Klein, M. L. *Phys. Rev. Lett.* **1991,** *67,* 1763.

27. Mar, W.; Hautman, J.; Klein, M. L. *Comp. Mat. Sci.* **1995,** *3,* 481.

28. Koishi, T.; Yasuoka, K.; Ebisuzaki, T.; Yoo, S.; Zeng, X. C. *J. Chem. Phys.* **2005,** *123,* 204707.

29. Buehrle, J.; Herminghaus, S.; Mugele, F. *Phys. Rev. Lett.* **2003,** *91,* 086101.

30. Imano, A. M.; Beroual, A. *J. Colloid Interface Sci.* **2006,** *298,* 869.

31. Dzubiella, J.; Hansen, J.-P. *J. Chem. Phys.* **2004,** *121,* 5514.

32. Kane, D.; Daly, G. M.; El-Shall, M. S. *J. Phys. Chem.* **1995,** *99,* 7867.

33. Warshavsky, V. B.; Zeng, X. C. *Phys. Rev. Lett.* **2002,** *89,* 246104.

34. Luzar, A.; Svetina, S.; Zeks, B. *Chem. Phys. Lett.* **1983,** *96,* 485.

35. Lee, C. Y.; McCammmon, J. A.; Rossky, P. J. *J. Chem. Phys.* **1984,** *80,* 4448.

36. Luzar, A.; Svetina, S.; Zeks, B. *J. Chem. Phys.* **1985,** *82,* 5146.

37. Du, Q.; Freysz, E.; Shen, Y. R. *Science* **1994,** *264,* 826.

38. Shelley, J. C.; Patey, G. N. *Mol. Phys.* **1996,** *88,* 385.

39. Luzar, A.; Chandler, D. *Nature* **1996,** *379,* 55.

40. Liu, P.; Harder, E.; Berne, B. *J. Phys. Chem. B* **2005,** *109,* 2949.

41. Sato, M.; Kudo, N.; Saito, M. *IEEE Trans. Ind. Appl.* **1998,** *34,* 294.

42. DeGennes, P. G.; Badoz, J. *Fragile Objects;* Springer-Verlag: Berlin, 1996.

43. Zhang, X. Y.; Zhu, Y. X.; Granick, S. *Science* **2002,** *295,* 5555.

44. Hong, L.; Cacciuto, A.; Luijten, E.; Granick, S. *Nano Lett.* In press.

45. Lahann, J.; Mitragotri, S.; Tran, T.-N.; Kaido, H.; Sundaram, J.; Choi, I. S.; Hoffer, S.; Somorjai, G. A.; Langer, R. *Science* **2003,** *299,* 371.

46. Erbil, H. Y.; Demirel, A. L.; Avci, Y.; Mert, O. *Science* **2003,** *299,* 1377.

47. Uchida, K.; Izumi, N.; Sukata, S.; Kojima, Y.; Nakamura, S.; Irie, M. *Angew. Chem. Int. Ed.* **2006,** *45,* 6470.

48. Halle, B. *Phil. Trans. R. Soc. Lond. B* **2004,** *359,* 1207.

49. Langemann, D.; Krüger, M. *Math. Comput. Simulation* **2004,** *66,* 539.

50. Line tension is responsible for the increase in contact angle above the macroscopic value of 86°.[23]

Field characteristics	θ_c	θ_c, Ref.[23]
Zero field	$96.3 \pm 1.8^\circ$	95.3°[50]
$E_\perp = +0.03$ V/Å	$84.2 \pm 3.9^\circ$	
$E_\perp = -0.03$ V/Å	$89.9 \pm 1.5^\circ$	

Table 1: Measured contact angles from simulations of 2000 molecules of water on a graphite surface. Contact angles are expressed as averages of several individual trajectories, and quoted error limits are one standard deviation.

Field	interior	s-l	l-v	3-phase	edges
0.00	3.48,*3.51*	2.85,*2.95*	2.77	2.3	2.88,*2.94*
$+0.03_\perp$	3.46,*3.50*	2.91,*3.01*	2.78	2.4	NA
$-0.03_\perp$	3.47,*3.49*	2.75,*2.84*	2.78	2.2	NA
$+0.03_\parallel$	3.47,*3.50*	2.85	NA	NA	(2.79, 2.94),(*2.82,3.00*)

Table 2: The mean number of hydrogen bonds, $\langle n_{\rm HB} \rangle$, formed by each water molecule in different regions of the drop: drop interior, solid-liquid (s-l) interface, liquid-vapor (l-v) interface, 3 phase contact, and drop edges. The two values for the parallel field case refer to leading and trailing edges respectively. The imposed electric fields are in units of V/Å. Results are shown for geometric and energetic (*italic*) hydrogen bonding criteria taken from Refs. 39 and 40. Each region contains approximately the same number of molecules ($\approx$ 2 to 5% of the complete drop), except for the three phase contact line ($\approx$ 0.1% of the drop). The standard deviation in $\langle n_{\rm HB} \rangle$ is ± 0.01.

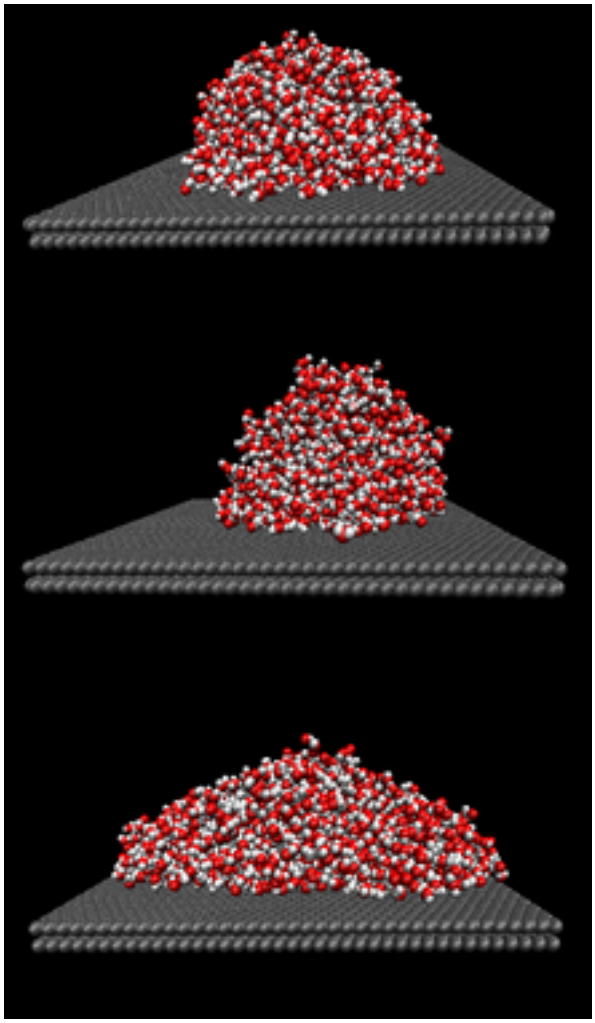

Figure 1: Snapshots of a 2000 molecule water droplet on a graphite surface. From top to bottom, drop in zero field, perpendicular field $E_\perp = 0.03$ V/Å and a parallel field $E_\parallel = 0.03$ V/Å.

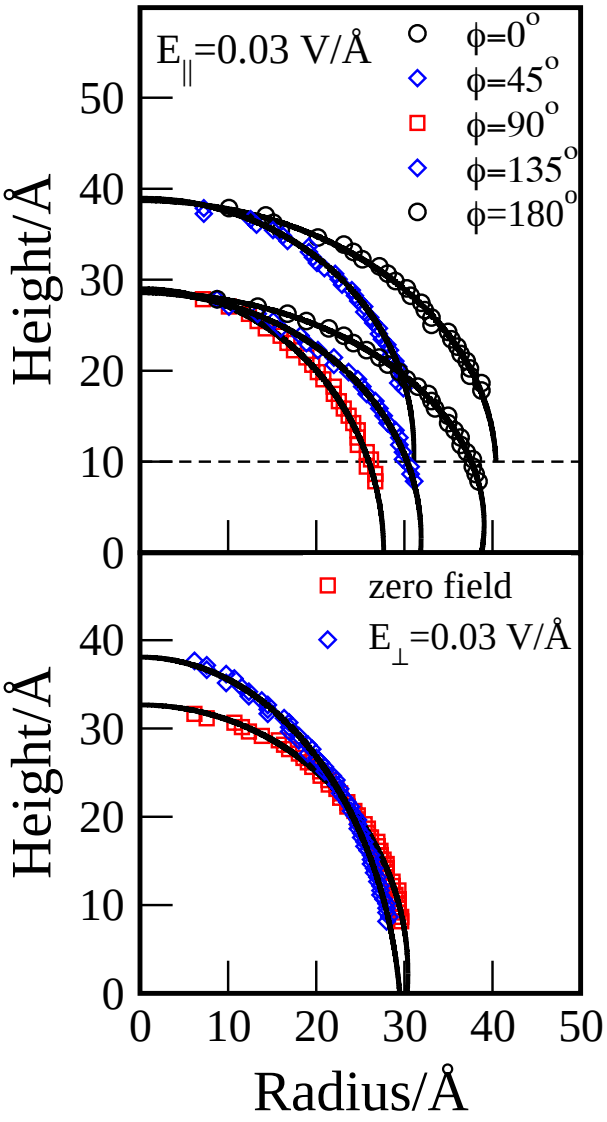

Figure 2: The vertical cross section of sessile water nanodroplets on graphite, showing elliptical sections (solid lines) fitted through simulation points (symbols). The bottom graph shows the drop in zero field and in perpendicular field $E_\perp = +0.03$ V/Å. The top graph shows the drop in parallel field $E_\parallel = 0.03$ V/Å at different values of the projection angle ϕ (see text), where the data for $\phi = 0°$ and $\phi = 45°$ have been vertically offset by 10 Å for clarity.

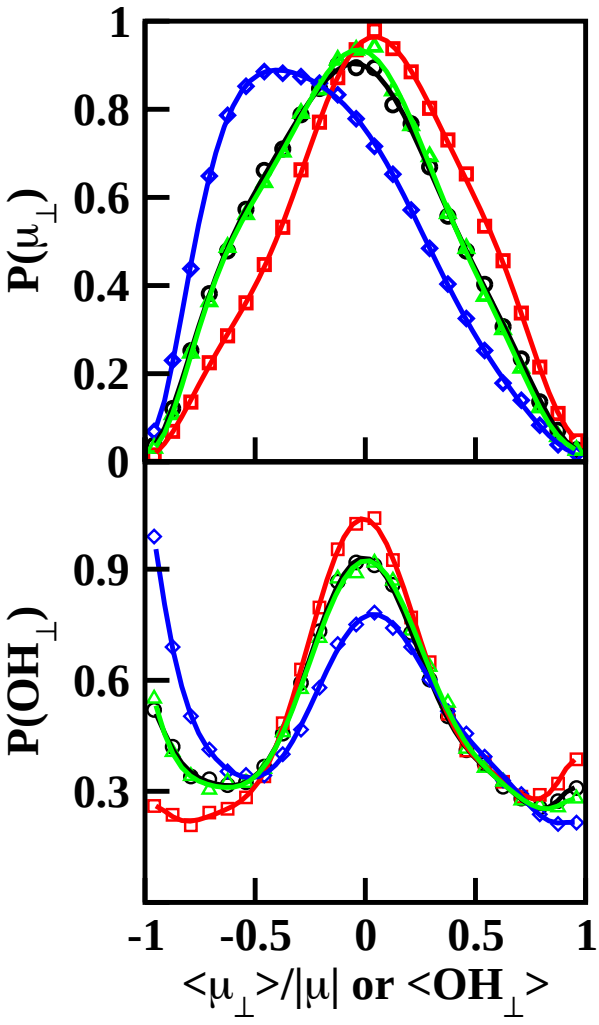

Figure 3: Distribution of perpendicular component of the water molecules' dipole moment vector $\boldsymbol{\mu}$ (top) and $\vec{\mathrm{OH}}$ vector (bottom) near the water-graphite interface. Black circles and line are in zero field. Red squares and line are in a perpendicular field $E_\perp = 0.03$ V/Å. The blue diamonds and line are in a perpendicular field $E_\perp = -0.03$ V/Å. The green triangles and line are in a parallel field $E_\parallel = 0.03$ V/Å.